Supplementary Information

Frustrated Rotations in Single Molecule Junctions

Young S. Park[1,2], Jonathan R. Widawsky[2,3], Maria Kamenetska[2,3], Michael L. Steigerwald[1], Mark S. Hybertsen[4], Colin Nuckolls[1,2], Latha Venkataraman[2,3]

[1]Department of Chemistry, Columbia University, New York, NY

[2]Center for Electron Transport in Molecular Nanostructures, Columbia University, New York, NY

[3]Department of Applied Physics and Applied Mathematics, Columbia University, New York, NY

[4]Center for Functional Nanomaterials, Brookhaven National Labs, Upton, NY

Content:

Synthetic Procedures:

All reactions were carried out in oven-dried glassware under argon atmosphere. Anhydrous and anaerobic solvents were obtained from a Schlenk manifold with purification columns packed with activated alumina and supported copper catalyst (Glass Contour, Irvine, CA). Every solution addition or transfer was performed with syringes. Chromatographic purifications were performed on a CombiFlash® R_f system using RediSep® R_f normal phase silica columns (Teledyne ISCO, Inc., Lincoln, NE). ^{1}H NMR (300MHz) and ^{13}C NMR (75MHz) spectra were recorded on a Bruker DRX-300 spectrometer at room temperature. High resolution mass spectra (HRMS) were recorded on a JEOL JMSHX110A/110A tandem mass spectrometer. Benzo[1,2-*b*:4,5-*b'*]dithiophene, benzo[1,2-*b*:4,5-*b'*]diselenophene, and $[Ru(NCMe)_3(triphos)](BPh_4)_2$ were prepared according to literature procedures[1]. All other starting materials were purchased from commercial sources. All the compounds for conductance measurements were further purified by recrystallization.

1,4-Bis(methylthio)benzene (1)

To a stirred solution of 1,4-dibromobenzene (1.18g, 5.0mmol) in dry THF (50mL) at -78^{o}C was slowly added *tert*-butyllithium (1.7M in pentane, 11.8mL, 20mmol). After 30min, the temperature was allowed to rise to room temperature. Elemental sulfur powder (0.337g, 10.5mmol) was then added in one portion, and the resulting mixture was stirred for 30min. After addition of methyl iodide (0.65mL, 10.4mmol) in dry THF (2mL), the mixture was further stirred for 1hr. The solvent was evaporated and the residue was dissolved in CH_2Cl_2 and washed with water. The organic phase was separated, dried over anhydrous $MgSO_4$, and concentrated in vacuo. The residue was purified by column chromatography to give white solids (0.49g, 58%).
^{1}H NMR (300MHz, $CDCl_3$) δ 2.49 (s, 6H), 7.22 (s, 4H). ^{13}C NMR (75MHz, $CDCl_3$) δ 16.81, 128.07, 135.60. HRMS calculated for $C_8H_{10}S_2$: 170.0224 found: 170.0224.

1,4-Bis(methylseleno)benzene (2)
Compound **2** was prepared from 1,4-dibromobenzene (1.18g, 5.0mmol) and selenium powder (0.829g, 10.5mmol) by a similar reaction (0.57g, 43%).
^{1}H NMR (300MHz, $CDCl_3$) δ 2.37 (s, 6H), 7.35 (s, 4H). ^{13}C NMR (75MHz, $CDCl_3$) δ 7.88, 130.05, 131.65. HRMS calculated for $C_8H_{10}Se_2$ ($^{80}Se_2$): 265.9115 found: 265.9115.

2,3,6,7-Tetrahydrobenzo[1,2-*b*:4,5-*b'*]dithiophene (3)
A solution of $[Ru(NCMe)_3(triphos)](BPh_4)_2$ (0.030g, 0.020mmol) and benzo[1,2-*b*:4,5-*b'*]dithiophene (0.077g, 0.40mmol) in THF (20mL) was placed into the reaction vessel and pressurized with hydrogen to 50psi at room temperature. The reaction vessel was heated to 60^{o}C with stirring. After 24h, the reaction mixture was cooled to room temperature and depressurized. The reaction mixture was filtered through a pad of silica and washed with THF (2x20mL). The solution was concentrated in vacuo and purified by column chromatography to give white solids (0.031g, 39%).
^{1}H NMR (300MHz, $CDCl_3$) δ 3.22 (t, *J* =1.5Hz, 4H), 3.40 (t, *J* =1.5Hz, 4H), 7.07 (s, 2H). ^{13}C NMR (75MHz, $CDCl_3$) δ 34.26, 36.35, 118.62, 137.63, 139.97. HRMS calculated for $C_{10}H_{10}S_2$: 194.0224 found: 194.0215.

2,3,6,7-Tetrahydrobenzo[1,2-*b*:4,5-*b'*]diselenophene (4)
Compound **4** was prepared from benzo[1,2-*b*:4,5-*b'*]diselenophene (0.20g, 0.70mmol) by a similar reaction (0.12g, 59%).
^{1}H NMR (300MHz, $CDCl_3$) δ 3.33 (t, *J* =5.7Hz, 4H), 3.42 (t, *J* =5.7Hz, 4H), 7.17 (s, 2H). ^{13}C NMR (75MHz, $CDCl_3$) δ 27.40, 38.70, 122.46, 133.67, 143.10. HRMS calculated for $C_{10}H_{10}Se_2$ ($^{80}Se_2$): 289.9115 found: 289.9104.

Measurement and Data Analysis:
The details of our experimental apparatus has been described previously[2]. Briefly, the STM was constructed from a home-built tip holder mounted on top of a single-axis piezoelectric positioner (Mad City Labs). A bias was applied between a cut Au wire tip and an Au substrate placed on top of the piezoelectric positioner and the resulting current was converted to a voltage with a current amplifier (Keithley 428). Data collection and control of the piezoelectric positioner were done by means of a data acquisition board (National Instruments, PXI-4461) driven by a customized program using Igor software (Wavemetrics Inc.) For the conductance trace measurements, the substrate approached the tip until a set conductance larger than G_0 was measured to ensure that the Au/molecule/Au junction from the previous measurement was completely destroyed. The sample was then withdrawn at a rate of 15 nm/s and the current and position data was recorded at a 40 kHz sampling frequency.

Histograms were constructed from the current versus position traces by converting currents to conductances and binning the data as a function of conductance using linear bins, and without any data selection. The most probable molecular junction conductance values for **3** and **4** were determined from a Lorentzian fits to the histograms with functional form: $f(G) = A/((G-G_{peak})^2+B^2)$. Here, G_{peak} is the peak conductance. For both molecules, the histograms for 10 sets of 1000 traces each were individually fit with a Lorentzian to determine $G_{peak.}$ The molecule conductance reported is the mean of the

G_{peak} values from all the fits for each molecule. The error bar is the standard deviation of the G_{peak} values.

For step length measurements, the custom piezoelectric positioner has a built in position sensor calibrated by the manufacturer, which has sub-angstrom accuracy. In addition, we have calibrated the piezo using interference measurements, and find the absolute values of the measured displacements to be accurate to within 5%.

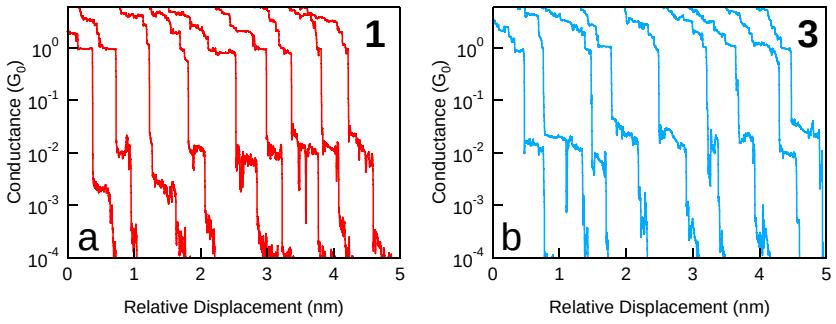

*Figure S1: Sample conductance traces measured with molecule **1** and **3**.*

The molecular junction step lengths were determined by an automated fitting algorithm. For each measured trace, the derivative of the logarithm of the trace was computed. Traces with peaks in the derivative that crossed a fixed threshold were considered further. The average conductance from the raw data in the region between two successive peaks was computed. (See Figure S2). Traces were considered to have molecular steps if this average conductance was within the peak region in the conductance histogram and if this region had more than 5 data points. Steps that had fewer than 5 data points, or equivalently those that were shorter than 0.007 nm were not included in the analysis. The average conductance for the step was calculated. The step was also fit with a line and its slope and length was determined. If traces had multiple steps within the same conductance region, the sum of the lengths of the individual steps was used as a total step length. Step length distributions for all four molecules are shown in Figure S3.

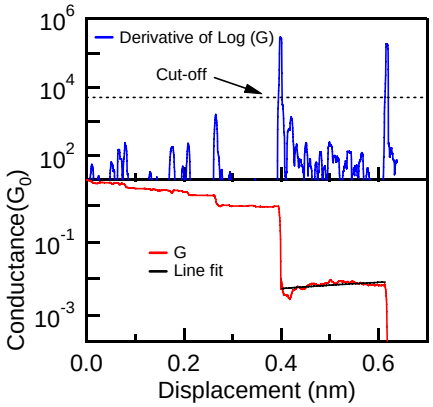

Figure S2: A sample conductance trace (lower panel) and the derivative of the log of the trace (upper panel).

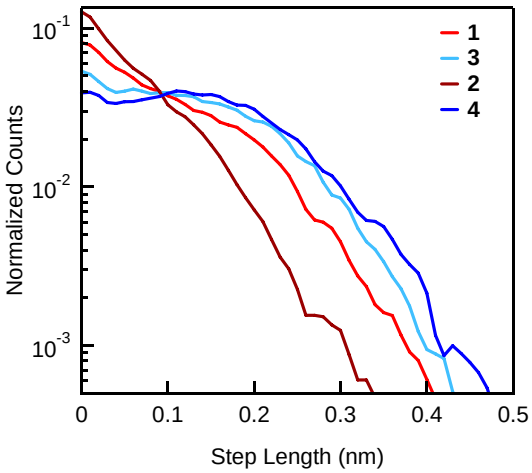

Figure S3: Step length distribution for all molecules studied here shown on a semi-log scale.

The average conductance value from each step was used to construct the histograms shown in Figure 2A. The peak position of these histograms was determined by fitting a Gaussian to the top portion of the histograms. The error bars in these values are the width of the bins used for the histograms. The peak in these histograms represent the most frequently observed step average conductance, with each step contributing one value to the histogram, as opposed to the full histograms of Figure 1B, where the entire trace has been used to construct the histogram. The peak position in the step average histogram need not occur at the same position as the peak in the full histogram. In an ideal case when the junction conductance is exactly the same for all junctions measured, and each trace has a completely flat step, these two methods will yield exactly the same number. However, when conductance varies from trace to trace and within a trace, the step-average conductance will generally differ from the 'most-probable" conductance.

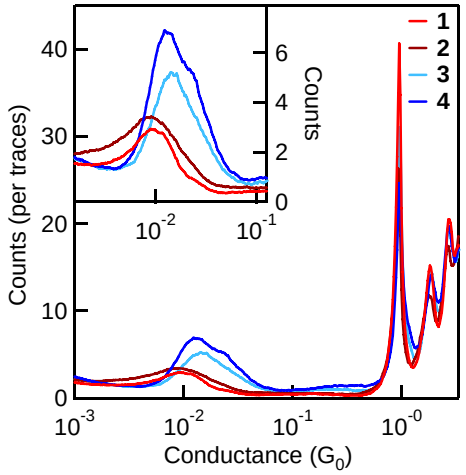

Figure S4: Logarithm binned conductance histograms constructed from all data, using 100 bins per decade. Inset shows the molecular peak region.

Logarithm binned histograms are also constructed for all molecules by taking the base 10 logarithm of the entire conductance trace and binning the data using 100 bins per decade. These are shown in Figure S4 for all four molecules measured. We can see clear

peaks for all molecules, at positions very close to those seen in Figure 2A. However, compared to a linear binned histogram, one skews the probability distributions of the conductance values by using log-binning. As a result, the log binning procedure can sometimes generate a peak in the histogram when a peak is not visible in a linear binned histogram. Mathematically this occurs because the number of counts per bin is increased systematically for higher conductance regions relative to lower conductance regions[3].

Theoretical Procedures:

The DFT results presented were based on the generalized gradient approximation (GGA) as formulated by Perdew, Burke and Ernzerhof (PBE).[4] We also performed calculations with the hybrid B3LYP functional for comparison[5]. The molecular calculations were done with Jaguar v7.5[6] using a 6-31g** basis for the light atoms and a lacvp** basis for Au.[7] The molecular geometry was fully relaxed. The final results for the binding energy were obtained with single point calculations using a 6-311g** and a lacv3p** basis respectively. Each S-Au link was modeled using Au clusters ranging from a single atom up to five atoms. To specifically simulate an undercoordinated Au contact atom on a close-packed Au contact, we focus on the Au_5 model shown in Figure S3 with four Au atoms frozen in a fragment of the fcc packing arrangement from metallic Au and an unconstrained Au atom initially located in the environment of an hcp hollow site on an Au(111) facet. Test calculations of binding were also performed with 20 atom clusters based on four layer (111) oriented pyramids. The PBE based binding energy is relatively consistent going from Au_1 to Au_5 and finally Au_{20} cluster models (<0.1 eV per bond variation), while the B3LYP binding energy shows more variation and somewhat weaker binding (about 0.2 eV per bond for the Au_{20} model).

The torsional angle energy landscape was probed using the Au_5 clusters to simulate the tip and substrate, with Ci symmetry imposed. The separation between tip and substrate was optimized before making the torsional angle scan, corresponding to a near zero applied force condition. The optimized torsion angle is about 88 degrees. At each step the scan, the natural torsion around the S-C bond was fixed, allowing all other degrees of freedom to relax, except the frozen Au atoms in each tip.

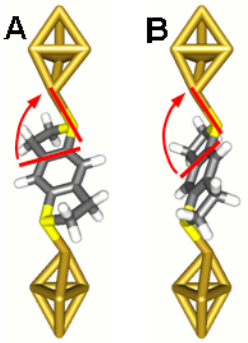

*Figure S5. Illustration of model junctions formed with **3** and Au_5 clusters. (a) 70 degree torsion. (b) 108 degree torsion.*

Reference:

(1) Takimiya, K.; Konda, Y.; Ebata, H.; Niihara, N.; Otsubo, T., *J. Org. Chem.* **2005,** 70, (25), 10569-10571; Duliere, E.; Devillers, M.; Marchand-Brynaert, J., *Organometallics* **2003,** 22, (4), 804-811; Rhodes, L. F.; Sorato, C.; Venanzi, L. M.; Bachechi, F., *Inorg. Chem.* **1988,** 27, (4), 604-610; Bianchini, C.; Meli, A.; Moneti, S.; Vizza, F., *Organometallics* **1998,** 17, (12), 2636-2645.
(2) Ulrich, J.; Esrail, D.; Pontius, W.; Venkataraman, L.; Millar, D.; Doerrer, L. H., *J. Phys. Chem. B* **2006,** 110, (6), 2462-2466; Venkataraman, L.; Klare, J. E.; Tam, I. W.; Nuckolls, C.; Hybertsen, M. S.; Steigerwald, M. L., *Nano Lett.* **2006,** 6, (3), 458 - 462.
(3) Hybertsen, M. S.; Venkataraman, L.; Klare, J. E.; Whalley, A. C.; Steigerwald, M. L.; Nuckolls, C., *J. Phys.: Condens. Matter* **2008,** 20, (37), 374115.
(4) Perdew, J. P.; Burke, K.; Ernzerhof, M., *Phys. Rev. Lett.* **1996,** 77, (18), 3865-3868.
(5) Becke, A. D., *J. Chem. Phys.* **1993,** 98, (7), 5648-5652.
(6) *Jaguar 7.5*, Schrodinger, L.L.C., New York, NY 2008.
(7) Wadt, W. R.; Hay, P. J., *J. Chem. Phys.* **1985,** 82, (1), 284-298.